Evolution Letters, 2024, **8**(5), 695–704
https://doi.org/10.1093/evlett/qrae024
Letter

Experimental evolution of multicellularity via cuboidal cell packing in fission yeast

Rozenn M. Pineau[1,2], Penelope C. Kahn[3], Dung T. Lac[1], Tom E. R. Belpaire[4], Mia G. Denning[1], Whitney Wong[1], William C. Ratcliff[1], G. Ozan Bozdag[1]

[1]School of Biological Sciences, Georgia Institute of Technology, Atlanta, GA, United States
[2]Interdisciplinary Graduate Program in Quantitative Biosciences, Georgia Institute of Technology, Atlanta, GA, United States
[3]Department of Zoology, University of British Columbia, Vancouver, Canada
[4]Division of Mechatronics, Biostatistics, and Sensors, KU Leuven, Leuven, Belgium

Corresponding author: School of Biological Sciences, Georgia Institute of Technology, 30332 GA, United States.
Email: ratcliff@gatech.edu;gonensin.bozdag@biology.gatech.edu

Abstract

The evolution of multicellularity represents a major transition in life's history, enabling the rise of complex organisms. Multicellular groups can evolve through multiple developmental modes, but a common step is the formation of permanent cell–cell attachments after division. The characteristics of the multicellular morphology that emerges have profound consequences for the subsequent evolution of a nascent multicellular lineage, but little prior work has investigated these dynamics directly. Here, we examine a widespread yet understudied emergent multicellular morphology: cuboidal packing. Extinct and extant multicellular organisms across the tree of life have evolved to form groups in which spherical cells divide but remain attached, forming approximately cubic subunits. To experimentally investigate the evolution of cuboidal cell packing, we used settling selection to favor the evolution of simple multicellularity in unicellular, spherical *Schizosaccharomyces pombe* yeast. Multicellular clusters with cuboidal organization rapidly evolved, displacing the unicellular ancestor. These clusters displayed key hallmarks of an evolutionary transition in individuality: groups possess an emergent life cycle driven by physical fracture, group size is heritable, and they respond to group-level selection via multicellular adaptation. In 2 out of 5 lineages, group formation was driven by mutations in the *ace2* gene, preventing daughter cell separation after division. Remarkably, *ace2* mutations also underlie the transition to multicellularity in *Saccharomyces cerevisiae* and *Candida glabrata*, lineages that last shared a common ancestor >300 million years ago. Our results provide insight into the evolution of cuboidal cell packing, an understudied multicellular morphology, and highlight the deeply convergent potential for a transition to multicellular individuality within fungi.

Keywords: multicellularity, cuboidal packing, convergent evolution, *Schizosaccharomyces pombe*

Lay Summary

Mother–daughter cellular adhesion is one of the most common ways that organisms evolve to form multicellular groups. Prior work with the snowflake yeast model system has shown that the physical constraints of cellular packing that result from mother–daughter adhesion can underpin the transition to multicellularity, allowing groups to become Darwinian entities capable of adaptation. However, it remains unclear whether this principle applies to other multicellular geometries arising from different mother–daughter cell adhesion patterns, such as those resulting from binary fission. In this paper, we investigate the origins of multicellularity via "cuboidal packing," a growth form found across the tree of life in which cells form groups composed of cubic subunits. We evolved unicellular spherical fission yeast with daily selection for larger group size, and multicellular groups with cuboidal packing rapidly evolved. These had an emergent multicellular life cycle through which groups grow and reproduce and in which group size was a heritable trait, allowing multicellular groups to become units of selection. Taken together, our work sheds light on the origin of multicellularity via cuboidal packing and demonstrates that the spontaneous origin of multicellular groups as Darwinian entities is not a feature of specific growth forms like snowflake yeast, but instead seems to be a general feature of mother–daughter cell adhesion.

Introduction

Multicellularity evolved dozens of times independently in different lineages, underscoring the diverse evolutionary paths that may lead to a multicellular life history (Grosberg & Strathmann, 2007; Umen & Herron, 2021). Over the last several decades, a broad range of work has highlighted just how influential the traits

Received November 07, 2023; revisions received March 21, 2024; accepted May 24, 2024

of the unicellular ancestor are during the transition to multicellularity (Bernardes et al., 2021; Olson & Nedelcu, 2016). For example, the evolution of cellular specialization is thought to arise via co-option of temporally varying cellular phenotypes, putting the unicellular toolkit to novel multicellular use (King et al., 2008; Kulkarni et al., 2022; Suga et al., 2013). Similarly, the morphology of multicellular groups is heavily dependent on the traits of the unicellular ancestor. How cells divide and attach to one another has fundamental consequences for the biophysical properties and evolutionary dynamics of these lineages (Day et al., 2022; Pentz et al., 2023).

In this paper, we focus on the early steps in the evolution of clonally developing multicellular morphologies, which result from the formation of permanent bonds between mother and daughter cells. If a cell can bud multiple times, remaining attached to each offspring, like the yeast *Saccharomyces cerevisiae*, then mother–daughter attachment results in branched groups with a tree-like morphology (e.g., snowflake yeast, Ratcliff et al. (2015), marine yeast, Mitchison-Field et al. (2019), algae, Niklas et al. (2019)). Alternatively, if the cells divide via binary fission and use the same division plane repeatedly, then permanent mother–daughter bonds result in linear filaments (e.g., *Nostoc*). If cells with binary fission instead have alternating division planes, then 3D structures with repeating cubic subunits of cells (composed of tetrads or octads) (Xiao et al., 2014) can result—a morphology that has been termed "cuboidal packing" (Xiao et al., 1998) (see Supplementary Figure S1 for a schematic of cuboidal packing).

Cuboidal packing has evolved repeatedly across the tree of life in both contemporary and ancient organisms (Figure 1A and B). For example, one of the most enigmatic macroscopic multicellular fossils from the Doushantuo Formation in southern China (570 MYA) forms large groups with cuboidally packed units (Figure 1A, panel 1). This species, which has been hypothesized to be an algae (Xiao et al., 1998), grows similarly to modern-day chlorosarcinacean green algae, like the lichen-forming green algae *Diplosphaera chodatii* (Figure 1A, panel 2). Cuboidal packing also appears within both the archaea and bacteria, for instance, in anaerobic methanogens and in the bacterial genus *Sarcina* spp. (*Methanosarcina* spp., Figure 1A, panel 3, *Sarcina* spp. Figure 1A, panel 4). While cuboidal packing is a relatively common route for group formation, no prior work has directly examined how it arises *de novo* and whether it can support an evolutionary transition in individuality in which groups of cells reproduce, possess heritable variation in emergent multicellular traits, and respond to group-level selection with multicellular adaptation.

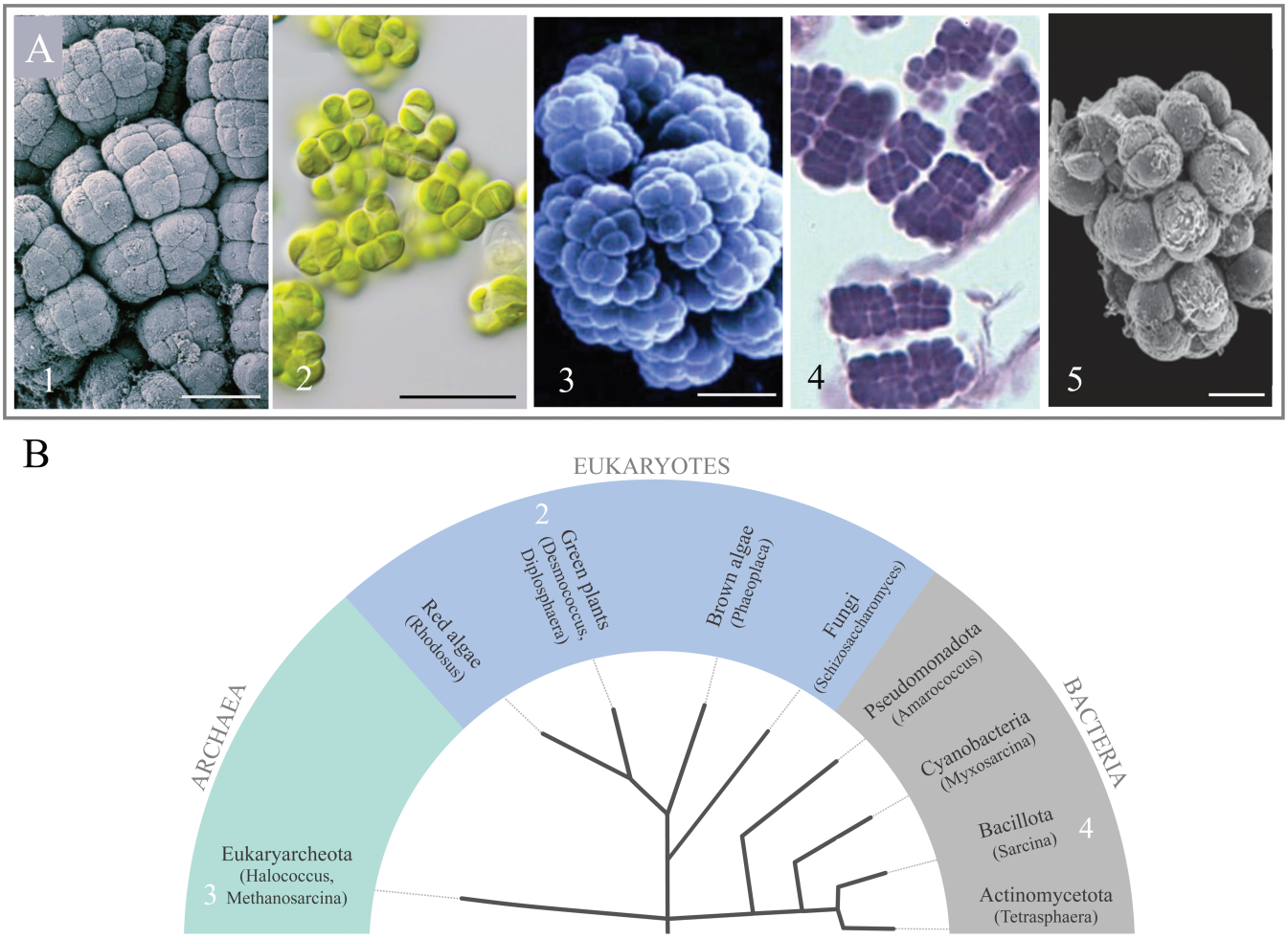

Figure 1. Cuboidal packing is found in all major branches of the tree of life. (A) Cuboidal packing has been observed in (1,5) fossils (Doushantuo algal thalli (Xiao et al., 1998), *Archeophycus yunnanensis* (Anderson et al., 2017)), and (2) extant eukaryotes (*Diplosphaera chodatii*) (Proeschold & Darienko, 2020), in (3) archaea (*Methanosarcina* spp.) (Whitehead Institute Center of Genome Research) and (4) bacteria (*Sarcina* spp.) (DiMaio et al., 2014). The scale bar is 20 μm. (B) Cladogram depicting the phylogenetic relationship of the examples above. See Supplementary Table S1 for details on these taxa.

Here, we investigate the evolution of cuboidal cell packing, a widespread yet understudied multicellular morphology, using spherical fission yeast as a model system. We subject these cells to settling selection, which favors larger group sizes, and observe the emergence of multicellular clusters with cuboidal organization within 20 rounds of selection (it is subsequently maintained until the end of the experiment, at 334 rounds of selection). We characterize the life cycle, heritability, and fitness of these clusters and show that they gain the capacity for multicellular adaptation, satisfying the key criteria for an evolutionary transition in individuality. We also identify the genetic basis of cluster formation and find that mutations in the *ace2* gene, which prevents cell separation after division, are responsible for this phenotype in two independent lineages. Our findings demonstrate that the evolution of cuboidal cell packing is driven by simple genetic and biophysical factors, leading to the emergence of multicellular Darwinian individuals. This morphology exhibits a remarkable degree of convergence across different lineages in the tree of life, highlighting the potential for this mechanism of group formation to underpin an evolutionary transition in individuality.

Methods

Evolution experiment

We applied daily settling selection to examine the evolution of nascent multicellularity in the haploid unicellular fission yeast, *Schizosaccharomyces pombe*. We started the selection experiment with an isogenic clonal ancestor of a spherical single-celled yeast (*sph2-3 ade3-58* h^{90}; Sipiczki et al., 2000). We selected this mutant for two key reasons: it did not naturally form multicellular clusters, and it had a random division plane orientation. We evolved five independent replicate populations in 5 ml YES media (0.5% (w/v) yeast extract, 3% (w/v) glucose, 225 mg/L adenine, histidine, leucine, uracil, and lysine). After every 24 hr of growth (30 °C, 220 rpm), we transferred 1 ml of the culture into a 2 ml Eppendorf tube. Following 5 min of settling through gravity, we discarded the top portion of the culture and transferred the bottom 25 μl into a fresh 5 ml YES culture to start the next round of growth and settling selection. We applied a 5-min settling selection for the first 190 days, followed by a more robust selection regime of 1-min settling selection until the final time point of 334 days. We made 30% glycerol stocks of each replicate population at approximately 15-day intervals and stored them at –80°C for further examination.

Measuring cluster biomass and area

To measure the increase in multicellular size, we picked single colony isolates from all five populations at t60, t125, and t344 (t = days). We then grew these isolates for three days with growth and settling selection, replicating the same conditions as our experimental evolution protocol. To measure the area of these evolved clusters, we diluted them 4,000-fold and pipetted these 15 samples into 24-well plates, then imaged the whole well with a Nikon Eclipse Ti microscope using 4× objective. Using custom-generated MatLab scripts, we measured the area of each cluster in microns, obtaining at least 3,000 cluster measurements per sample. Finally, to take visually appealing high-magnification images representing the ancestral and evolved *S. pombe* cells and clusters, we used a Nikon AR1 confocal microscope. For size distributions, we calculated a weighted mean, which accounts for the fact that unweighted means are heavily skewed by relatively small proportions of small groups like single cells (see Bozdag et al., 2023 for a detailed description of the method). This approach reports biomass-normalized size distributions, which can intuitively be thought of as the size of a group the average cell will be in.

Examining cell wall orientation via Fourier transform

Organisms growing with cuboidal packing have a characteristic "plus" shape to their cell walls, where tetrads of cells share cell walls. We examined this by fluorescently labeling cell walls and then performing a Fourier transformation on the resulting images. To stain the cell walls, we washed overnight cultures grown in 10 ml liquid YES once in dH_2O and twice in 1× PBS. We used calcofluor-white (CFW) using a final concentration of 50 μM with a 10-min incubation in the dark at room temperature. Following CFW staining, we washed the cells twice in 1× PBS before imaging.

We imaged CFW-stained yeast using a 20× objective on a Nikon A1R confocal microscope. To measure the angles of cell wall orientation, we applied the Fast Fourier Transform (FFT) to six separate images using ImageJ. The resulting FFT magnitude images were normalized with the mean magnitude of each image. We sampled the normalized FFT images over angles θ between 0 and 180 with steps of 1. For every angle, the normalized FFT images were integrated starting from the center of the image between –0.495W and 0.495W, where W is the full width of the image. If in fact multicellular *S. pombe* are growing as tetrads with connected cell walls forming a plus shape, then we expect to see the FFT peak at 90°. This approach is conservative, as we applied the FFT to whole images that include some out of plane cells, not ideal sub-sections showing the expected plus shape.

Time-lapse microscopy

To examine the growth and reproduction of evolved *S. pombe* clusters, we used time-lapse microscopy. Specifically, we first grew cultures overnight in 10 ml YES media. Next, we diluted them 10^3 and 10^4 times in 2× YES media combined with soft agar at a final concentration of 0.035%. We then pipetted 100 μl of a mixture of soft agar and clusters into 8-well chamber slides. We took images of the growing culture every 20 min for 24 hr using a 20× objective and across five different Z planes using a Nikon Eclipse Ti microscope. Finally, we processed these images using ImageJ.

Growth rate measurements

To examine the daily growth rate of evolved clusters, we revived all five frozen populations at t125 by growing them on YES plates. Then, single colony isolates from each population were grown to equilibrium for three days under their original growth conditions (liquid YES, with daily settling selection). We started recording the growth rate (t0 time point) after one round of settling selection. We then sampled the culture after 3, 6, 12, and 24 hr of growth. We estimated population size (number of clusters) and cluster size distribution for each time point in 24-well plates by imaging the whole well with a Nikon Eclipse Ti microscope using the 4× objective. Because the cluster size distribution is constant over the growth period (Figure 3B), the growth rate (fold change per unit time) of both cells and clusters will be very similar. We chose to measure the growth rate of groups, not cells, as our primary focus in this paper is on the origin of multicellular Darwinian entities, and most of our measurements in this paper are at this level.

Broad sense heritability

To measure broad sense heritability, we picked single isolates from all 5 lines at t60, t125, and t344 and cultured them for three days with growth and settling selection. We imaged the populations and measured the distribution of group size to estimate the

broad sense heritability of this trait (H^2) for specific hypothetical population compositions, as shown in Figure 3D. H^2 estimates the proportion of the total phenotypic variation in a population that is due to genetic differences. Following the procedure of van Kleunen et al. (2002), we parsed the variance components (VC) of genotype : $H^2 = VC_{genotype}/(VC_{genotype} + VC_{residual})$.

Measuring size-dependent fitness

To measure the effect of size on fitness during settling selection, we competed isolates from t60 versus t334 from line 3. To be able to perform colony plate counts and distinguish t60 from t334, we transformed t60 with hygromycin resistance (details below in the strain construction section). We mixed 750 μl of each strain and performed settling selection. We serial diluted the clusters and plated 1:4,000 and 1:8,000 dilutions for before and 1:2,000 and 1:4,000 for after settling selection on YES plates. After three days of growth, we counted the colonies and replica plated using velvet on YES+HYG plates. The plates were incubated for three more days before colony counting. Because both competitors decrease in frequency during settling selection, we estimate relative fitness with the following formula for the selection rate (r): $r = CFU_{t334\_ss}/CFU_{t334} - CFU_{t60\_ss}/CFU_{t60}$, with *CFU* standing for Colony Forming Units and *ss* denoting counts after settling selection.

Strain construction

To compete the t60 and t334 strains (Figure 3), we substituted the *ura4* gene with a hygromycin resistance cassette in a t60 strain isolate. Specifically, we inserted the hygromycin B resistance cassette at the *ura4* locus *ura4*Δ::*HYGMX* using the lithium acetate/dimethyl sulfoxide procedure outlined by Murray et al. (2016) and selected for mutants capable of growing on YES—hygromycin plates (see primers in Table 1).

To examine the phenotypic consequences of the loss of function in the *ace2* gene (Figure 4), we deleted the *ace2* open reading frame with a hygromycin resistance cassette. Using the same transformation protocol mentioned above, we inserted the hygromycin resistance cassette at the *ace2* locus *ace2*Δ::*HYGMX*, and selected transformants growing on YES—hygromycin plates (see Table 1 for primer sequences).

gDNA extraction and bioinformatic analysis

To identify candidate mutations for spherical cell shape and cluster formation, we sequenced clonal isolates of the unicellular ancestor and evolved clusters from five independent populations at t334. We used VWR's Life Science Yeast Genomic DNA Purification Kit to extract genomic DNA. We then mailed the genomic DNA samples to the Microbial Genome Sequencing Center (SeqCenter, https://www.seqcenter.com/) for library preparation and Illumina sequencing.

Table 1. Primer sequences used to knock out Ura4 (see Figure 3) and Ace2 (see Figure 4) with insertion of the hygromycin resistance cassette. Uppercase letters correspond to the gene-matching primer sequences, and lowercase letters correspond to plasmid-matching sequences.

Primer	Sequence
URA4-F	CCGTATTGTCCTACCAAGAACCTCTTTTTTGCTTGGATCG AAATTAAAGGTTTAAAAGCAAAGTTcgtacgctgcaggtcgac
URA4-R	CAAACGCAAACAAGGCATCGACTTTTTCAATAACCAACC AAAAAAATTTTACATTAGTCTTTTTatcgatgaattcgagctcg
ACE-F	CAAAGAAATCTATAGGACCAAAAACGGTGTT AATACAATCcgtacgctgcaggtcgac
ACE-R	ATTATTTACTATGTTAATATCATGCATAGATA AATGTTCGatcgatgaattcgagctcg

We analyzed 150-bp paired-end Illumina reads on a Linux platform. First, we used FASTP (v.0.21.0; Chen et al., 2018) to trim the first 15 and the last cycles of the sequencing run and filter out reads lower than a PHRED score of 30. We aligned reads to the most recent version of the *S. pombe* reference genome (https://www.pombase.org/data/genome_sequence_and_features/genome_sequence/) using BWA-MEM (v.0.7.17; Li, 2013). Next, to sort, index, and convert SAM files to BAM files and to mark the duplicates, we used PICARD tools (v.2.24.0, http://broadinstitute.github.io/picard/), SAMTOOLS (v.1.7; Li et al., 2009), and BAMTOOLS (v.2.3.0; Barnett et al., 2011). We then used GATK's ValidateSamFiles and HaplotypeCaller tools (v.4.1.9.0) to validate BAM files and call variants Van der Auwera et al. (2013). Next, we used VCFtools (v.0.1.17; Danecek et al., 2021) to filter out variants with a PHRED score lower than 30, a minimal depth below 12, and an allele frequency lower than 0.1. We then identified de novo variants unique to the evolved clusters using BCFTOOLS isec (v1.16). Finally, for a last round of filtering, we visually inspected VCF files on Integrative Genomics Viewer (IGV, v.2.8.13; Robinson et al., 2023) and removed variants at highly complex regions with alignment issues. We used SnpEff to predict the potential functional effects of the mutations (Cingolani et al., 2012). SnpEff is a genetic variant annotation tool that also provides an estimation of the strength of effect of the mutation. We identified candidate variants for the spherical cell shape by searching through the literature for known effects of the mutations detected in the sequenced ancestral strain (see Supplementary Table S2 for a complete list of the mutations). To search for GO terms associated with the putative mutations presented in Figure 4B, we generated a list of mutations that we ran in g:Profiler (Raudvere et al., 2019) tool to detect positive associations between mutations and the GO terms (Supplementary Table S3).

Results

Multicellular organisms with cuboidal packing typically have spherical cells (see Figure 1A). This may facilitate tetrad and octad formation by lowering geometric constraints on cellular packing. We thus started our experiment with a spherical mutant clonal isolate of the fission yeast *S. pombe*. This round mutant phenotype was obtained by screening for spherical mutants after UV radiation by Sipiczki et al. (2000). We sequenced its genome and identified a mutation on *gef1p* as a potential candidate mutation for sphericity. Gef1p activates a pathway for apical growth and to mediate cytokinesis that involves Cdc42, and mutations inactivating Cdc42 produce round spherical *S.pombe* cells (García et al., 2006, see Supplementary Table S2 for details on the mutations).

We evolved five replicate populations of initially clonal spherical *S. pombe* with daily settling selection for a total of 334 transfers—an experimental regimen shown to favor group formation in a range of organisms (snowflake yeast, Ratcliff et al., 2012; *Sphaeroforma arctica*, Dudin et al., 2022; *C. reinhardtii*, Ratcliff et al., 2013; *Kluyveromyces lactis*, Driscoll & Travisano, 2017). In brief, we grew 5 ml of culture for 24 hr and transferred a randomly subsampled 1 ml into a microcentrifuge tube. After a 5-min gravity settling selection, we discarded the top layer and transferred only the bottom 2.5% into a new 5 ml culture for the subsequent growth and settling phase (Figure 2A).

This approach simultaneously favors three traits essential for the evolution of multicellularity: first, settling selection favors group formation, as groups settle faster than single cells. Only

the fastest settling 2.5% of the sub-population's biomass is transferred, thus competition is an open-ended arms race (i.e., there is no size at which survival is guaranteed). Second, by discarding 80% of the population prior to settling selection, we maintain strong selection on there being a multicellular life cycle in which groups reproduce. That is, a lineage that simply grows indefinitely without reproducing will eventually be discarded, and it is an evolutionary dead end. Finally, the 24 hr of growth maintain strong selection for rapid growth. These traits may trade-off with one another and collectively ensure that we have created conditions under which groups that serve as multicellular Darwinian entities may arise.

Within 20 days of evolution, we observed the emergence of groups with a cuboidal packing morphology (Figure 2B), and by day 60 (~140 generations), the multicellular clusters had outcompeted their unicellular ancestor. To quantify cuboidal packing, we measured the cell–cell attachment angles by applying a Fourier transform to cell-wall stained confocal images (Figure 2C). We found that the most frequent angle is close to 90° (Figure 2D), which corresponds to perpendicular connections between cells. When cells divide, they remain attached to daughters at perpendicular angles, forming subunits composed of tetrads—a hallmark of cuboidal packing.

We observed a 567-fold increase in biomass-weighted mean cluster volume (an increase from 2.9 to 34.4 μm in biomass-weighted radius) within the first 60 days of the experiment, coinciding with the initial formation of multicellular groups. This was followed by a more gradual, 2-fold increase in group size over the remainder of the experiment from day 60 to day 334 (~790 generations total, Figure 2E). This increase in group size was significant (two-way ANOVA with time as a fixed effect and replicate population as a random effect, $F_{2,72789} = 3,454, p < 2 \times 10^{-16}$ for the effect of the time. All time points were different at $p < 0.01$ with Tukey's HSD).

To test whether spherical cell shape is important for the evolution of cuboidal packing, we also subjected the wild type *S. pombe*, which is rod-shaped, to settling selection for 60 days. In parallel, we deleted the gene *ace2* in the wild-type ancestor. While we observed the formation of multicellular clusters, they do not form cuboidal packets (Supplementary Figure S2), supporting our hypothesis, developed from the comparative record, that spherical cells are essential for cuboidal cell packing.

Next, we examined the capacity for these groups to serve as Darwinian individuals (Godfray & May, 2014; Godfrey-Smith et al., 2013). This occurs when groups reproduce, forming new groups, and there is heritable variation in group-level traits that affects fitness. When these conditions are met, multicellular Darwinian individuals can gain multicellular adaptations via natural selection, which can ultimately lead to the evolution of functionally integrated multicellular organisms (Rose & Hammerschmidt, 2021).

To explore the life cycle of multicellular *S. pombe*, which is required for groups to beget new groups, we imaged clusters from line 3 at t334 over a 24-hr period in soft agar. Clusters grew until a multicellular propagule separated from the main group via spontaneous fragmentation (Figure 3A), forming new groups from these propagules. Over 24 hr of growth in liquid media, their size distribution remained remarkably stable (mean radius of ≈15 μm over the 24 hr growth cycle, Figure 3B), while the number of clusters increased super-linearly (the mean growth rate was 0.13 clusters per hour across all five lines, Figure 3C). Multicellular *S. pombe* thus have an emergent multicellular life cycle generated by growth and reproduction, the latter driven by spontaneous fracture.

Next, to determine if the variation in group size is heritable, we measured the distribution of cluster size for isolates taken from all five replicate populations at three different time points (60, 125, and 334 days, which correspond to ~140, 300, and 790 generations, respectively) and calculated the broad sense heritability of group size, H^2 (Figure 3D) for all pairwise differences within lines (t60 vs. t125, t60 vs. t334, t125 vs. t334) using a variance partitioning approach. Broad sense heritability quantifies the proportion of the phenotypic variance in a population that can be attributed to genetic variance (see "Methods" section for equation). A value of 0 indicates that none of the observed variance in the trait is due to genetic factors, while a value of 1 suggests that all the variance is due to genetics. In extant clonally reproducing animals, H^2 is typically in the range of 0.3–0.75 (Spitze, 1993; Yund et al., 1997). Group size had a heritable component in most pairwise competitions, with H^2 ranging from 0.01% to 27% (Supplementary Figure S4, Figure 3D). The highest heritability estimates came from comparisons between t334 strains and their t60 ancestors, and, in general, H^2 scaled with the amount of evolutionary time separating two isolates.

Finally, to determine whether these heritable differences in cluster size grant a survival benefit during selection for multicellularity, we conducted a competition experiment between two strains with significant differences in size (i.e., 34 μm and 41 μm mean cluster radius for t60 and t334 isolates of line 3, respectively, see Figure 2E). In brief, we measured the frequency of each genotype before and after applying one round of settling selection. As a result, t334 clusters had an average of 6.7% higher fitness, measured as a selection rate constant (Lenski et al., 1991) across three replicate competitions (Figure 3E; $t_7 = 2.19$, $p = 0.045$, test of the intercept estimate of the selection rate coefficient in an ANOVA in which each of the four technical replicate fitness measurement is nested within the appropriate experimental replicate). Taken together (Figure 3A–E), our results demonstrate that evolved *S. pombe* clusters exhibit characteristics of Darwinian individuality: cuboidally packed clusters display a nascent multicellular life cycle that reproduces via multicellular propagules (Figure 3A–C), group size is heritable (Figure 3D), and these differences in multicellular size confer a survival advantage (Figure 3E). Perhaps most importantly, we see a sustained response to selection for larger size at the group level (Figure 2E).

To examine the genetic basis of cluster formation in *S. pombe*, we sequenced one isolate from each line from the latest time point of our evolution experiment (time 334). Two lines displayed mutations in the *ace2* gene: a loss of the start codon (line 2) and a frameshift mutation (line 3) (see Supplementary Table S4). Mutations in *ace2* also arose as a mechanism of group formation in response to similar selection in the budding yeast *S. cerevisiae* (Ratcliff et al., 2012, 2013). While both species are yeast, they are distantly related, having diverged 330–420 million years ago (Sipiczki, 2000). This observation exemplifies a case of convergent evolution despite a deep temporal divergence. When we knocked out *ace2* in the unicellular *S. pombe* ancestor, we observed the emergence of multicellular clusters (Figure 4A). This mutation alone is not sufficient to fully recapitulate the evolved phenotype: while it formed groups with a biomass-weighted mean volume 82 times greater than the unicellular ancestor, this was still just 6% of the size of 60-day evolved strains (mean radius of the unicellular ancestor = 2.9 μm, mean radius of *ace2*Δ= 12.9 μm, mean radius of 60-day evolved clusters across the five lines = 32.8 μm, all differences

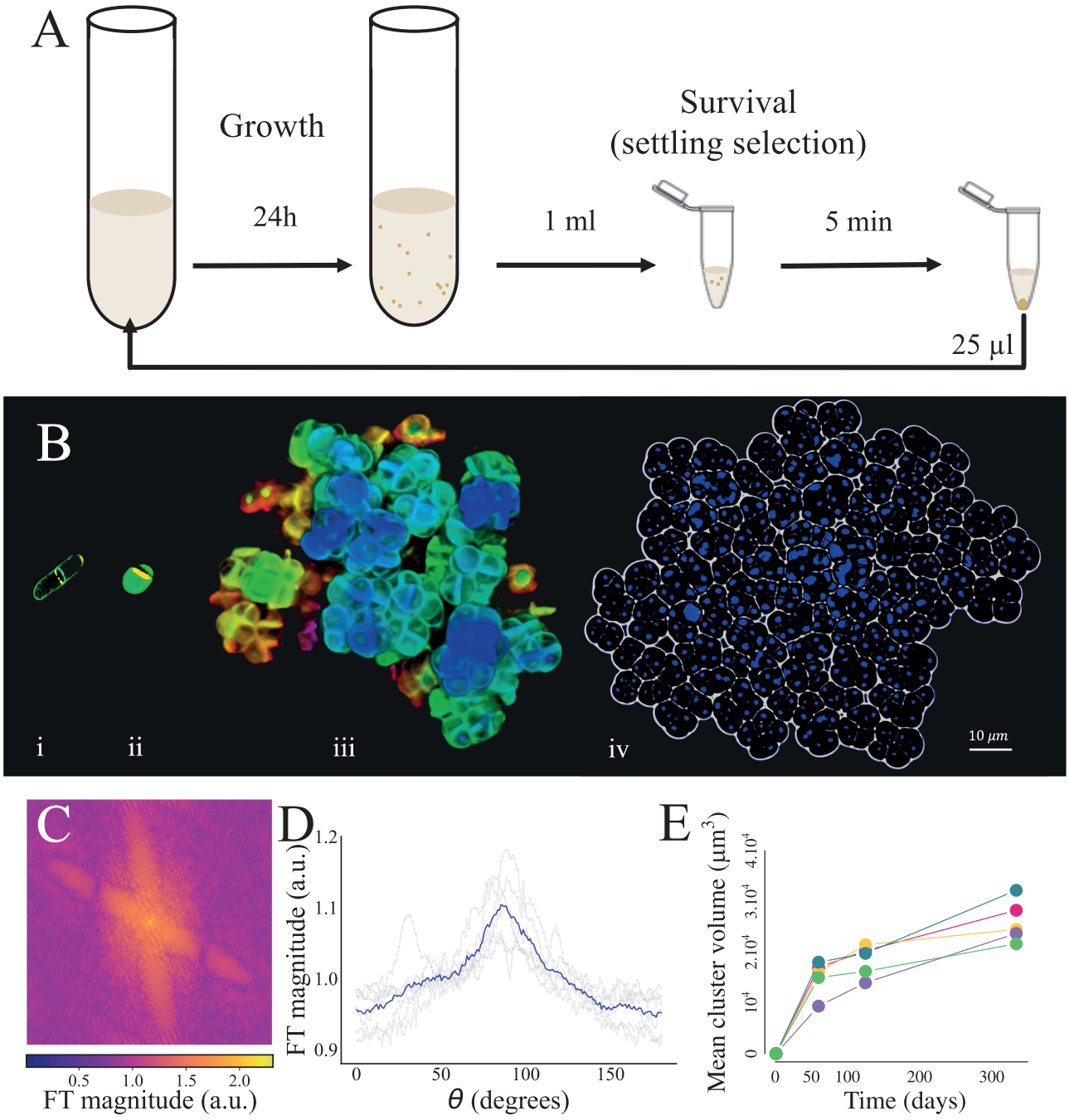

Figure 2. Emergence of multicellular groups in spherical fission yeast. (A) Culture cycle. Each day, *S. pombe* was grown for 24 hr before being subject to settling selection for larger size. (B) Cuboidally packed multicellular groups evolved within 20 days. The image shows the wild-type ancestor (i), the spherical single-celled mutant (ii), day-85 multicellular *S. pombe* in confocal microscopy (iii), and fluorescence microscopy (iv) with DAPI-stained nuclei. Colors in (i–iii) represent depth in z-position. See Supplementary Figure S3 for images of whole populations for the five independently evolving lines. (C) To quantify cuboidal packing, we performed Fourier analysis on confocal images of fluorescently labeled cell walls. (D) The highest angle frequency of the Fourier transform is approximately 90°, capturing the characteristic "plus sign" shape of shared cell walls in tetrads of cells. (E) The biomass-weighted mean volume of the clusters increased by a factor of 567 in the first 60 days (~140 generations), reflecting the origin of multicellular groups, which was followed by a slower increase (2-fold from day 60 to 334, ~790 generations total).

were significant with $p < 0.001$ via Tukey's HSD after one-way ANOVA, $F_{2,4395} = 5,977, p < 2 \times 10^{-16}$).

GO enrichment analysis on the set of mutations highlighted genes involved in autophagy, cell growth, and in pathways like the target of rapamycin complex 1 (Torc1) (Figure 4B). For instance, two lines independently evolved mutations in *hhp1* (lines 2 and 4) and in *tor2* (lines 1 and 3). These genes code for serine/threonine protein kinases that could influence cell growth. Additionally, lines 1 and 5 possessed a mutation in *exg1* gene, a cell wall glucan involved in cell wall organization or biogenesis, which may be involved in cellular adhesion. However, further work will be required to determine what role, if any, these mutations have in the evolution of multicellularity via cuboidal packing in our system.

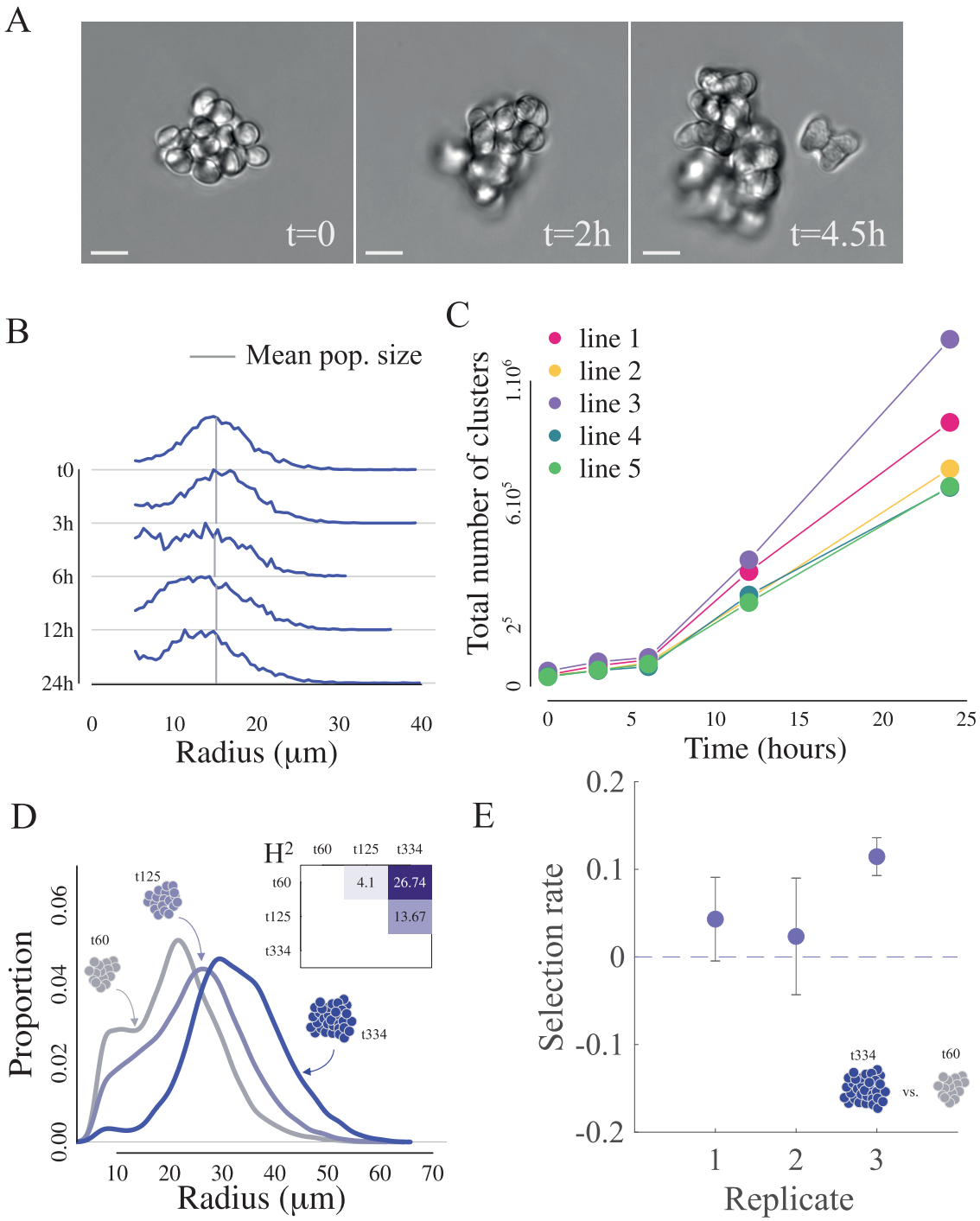

Figure 3. Multicellular *S. pombe* have an emergent multicellular life cycle in which groups become units of selection. (A) *S. pombe* clusters fracture during growth, even without mechanical strain from mixing, producing propagules in soft agar (full time-lapse video in supplementary material, scale bar is 10 μm). (B) The size distribution of the population remains stable over the 24-hr period of growth, during which (C) there is a lag phase followed by a sharp increase in cluster number. (D) Size is heritable: we measured the broad sense heritability (H^2) in all-pairwise comparisons between three time points (t60, t125, and t334, see inset). See Supplementary Figure S4 for heritability values for all lines. (E) Group size affects fitness: when subjected to settling selection, larger groups (i.e., evolved clusters at t334) do, on average, 6% better than smaller groups (i.e., evolved clusters at t60). All experiments in this figure were conducted using line 3. Bars represent standard error of the mean for four replicate fitness measures of the same competition.

Discussion

Cuboidal cell packing is a common yet understudied multicellular morphology that has evolved independently in diverse lineages, from ancient fossils to modern algae, bacteria, and archaea. Previous studies have suggested that cuboidal cell packing may arise from spherical unicellular ancestors that divide by binary fission and alternate their division planes (Xiao et al., 1998). However, no prior work has directly examined how this topology arises

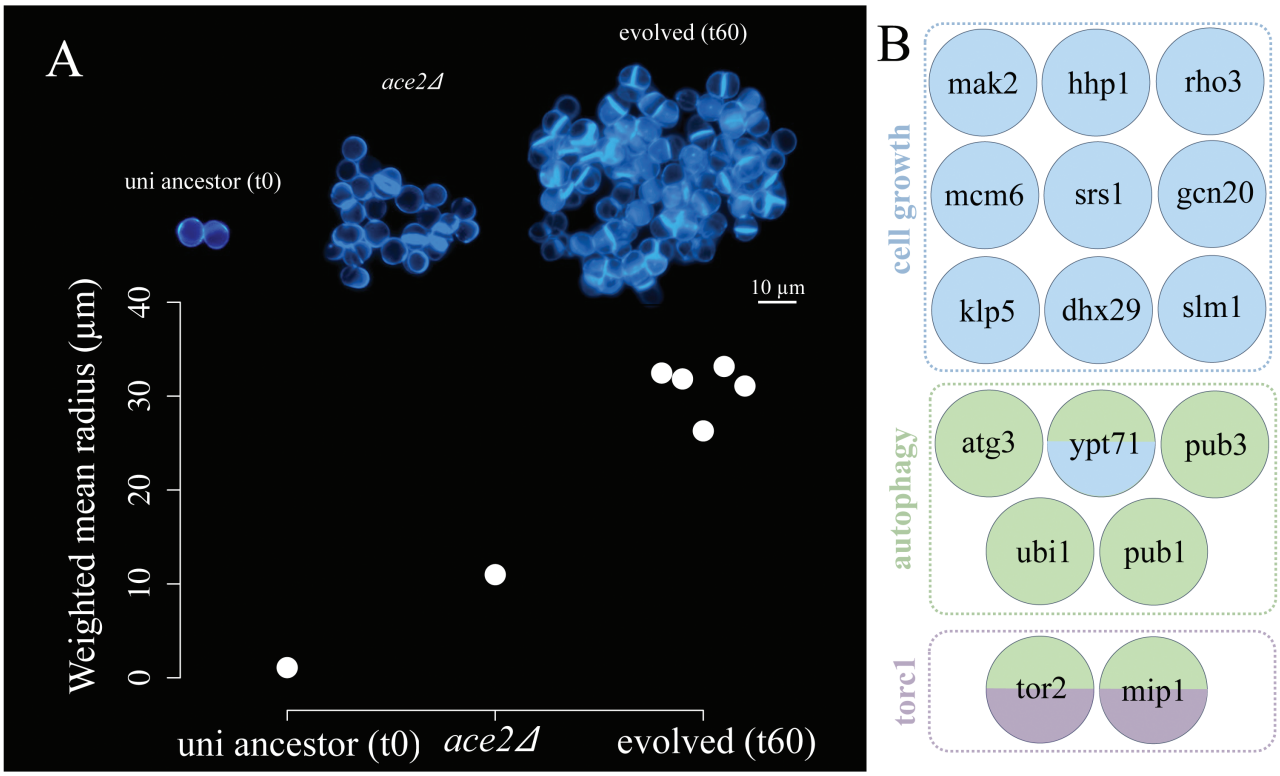

Figure 4. Genetics of multicellular *S. pombe*. (A) We found missense mutations in *ace2* in two independently evolved lines (lines 2 and 3). Loss-of-function mutations in *ace2* resulted in the formation of small multicellular clusters, but did not fully recapitulate the evolved phenotype (mean radius size for t60 evolved lines). Confocal images show unicellular ancestor, *ace2* knockout mutant in the unicellular ancestor background, and 60-day evolved cluster from line 3. Scale bar is 10 μm. (B) The GO enrichment analysis identified mutations involved in cell growth, autophagy, and the *torc1* complex. *ypt71* is in both 'cell growth' and 'autophagy' GO categories; *tor2* and *mip1* are in both 'autophagy' and '*torc1*' GO categories.

de novo, and whether it can support an evolutionary transition in individuality. Here, we used spherical fission yeast as a model system to experimentally evolve cuboidal cell packing under settling selection, which favors larger size. We chose fission yeast because they are genetically tractable, have a short generation time, and can be easily manipulated to produce spherical cells by mutating genes involved in cell shape determination (Sipiczki et al., 2000).

We observed the emergence of multicellular clusters with cuboidal organization within 20 rounds of selection, displacing the unicellular ancestor. These clusters displayed key hallmarks of an evolutionary transition in individuality: groups possessed an emergent life cycle, their size was heritable, and they responded to group-level selection via multicellular adaptation. The size distribution of the population was remarkably stable, even as the population size increased super-linearly. Combined with our observation of spontaneous fracture during growth (Figure 3A), this suggests that fracture is driven by cell–cell strain accumulation during growth, as has previously been shown in snowflake yeast (Jacobeen et al., 2018). Like snowflake yeast, this life cycle arises "for free" as an emergent property of cellular crowding during growth.

Two out of five replicate populations had loss of function mutations in the gene *ace2*. This is similar to what was seen with budding yeast, *S. cerevisiae*, when it was evolved under the same selective regime: 50% (5/10) of the replicate lines gained loss-of-function mutations in *ace2* (Ratcliff et al., 2015). These fungal species last shared a common ancestor 330–420 million years ago (Sipiczki, 2000) and have deeply divergent cell biology. This observation exemplifies a case of convergent evolution over at both phenotypic and genotypic levels. Moreover, *ace2* mutations also induce multicellular group formation in *Candida glabrata* (Kamran et al., 2004), another species of budding yeast that is as divergent from *S. cerevisiae* as humans are from fish. *ace2* plays a conserved role in regulating cytokinesis across the Ascomycota, so perhaps it is not surprising that it would play a similar role in such distantly related organisms.

The convergently evolving loss of function mutations in *ace2* highlights the powerful historical contingency exerted by the unicellular ancestor's cell biology on the mechanisms and dynamics of multicellular evolution. And yet, despite a similar mechanism of group formation (mother–daughter adhesion due to incomplete cytokinesis), budding and fission yeast generate remarkably different multicellular morphologies: budding generates fractal trees, while binary fission generates groups with cuboidal packing. While both topologies generate an emergent multicellular life cycle that allows groups of cells to become Darwinian individuals, little is known about how these early, yet fundamental, differences in group formation will affect their subsequent multicellular evolution.

Some early clues have emerged from ongoing evolution experiments: over 600 transfers with daily settling selection, snowflake yeast evolved to be >20,000-fold larger and >10,000-fold more mechanically tough. They accomplished this by evolving novel biomechanics that leverage their branching phenotype: the evolution of elongate cells reduced the accumulation of cell–cell strain (which, when it gets large enough, breaks a mother–daughter bond and breaks the group, Bozdag et al., 2023). When combined with mutations strengthening connections between cells, groups

withstood fracture long enough that the cells began to grow around one another, ultimately entangling. Through entanglement, which requires many bonds to be broken before a propagule is separated, snowflake yeast leveraged their specific multicellular morphology to drive considerable multicellular trait innovation. It is unclear whether organisms with cuboidal packing can evolve to form large, mechanically tough groups. Consistent with the relatively small size achieved in our experiment here, most extant multicellular organisms with this growth form remain small and simple (though *Archaeophycus*, Figure 1A, panel 5, is a notable counter-example). Entanglement, which has evolved readily in organisms with a branching morphology, does not appear to be possible in an organism composed of cuboidal subunits. Whether, relative to other multicellular topologies, cuboidal packing faces stronger mechanical constraints on size and toughness and how this relates to the evolution of multicellularity complexity more broadly remain open questions (Knoll, 2011).

Conclusion

In this paper, we explore the evolution of multicellularity through cuboidal packing, a form of clonal multicellularity in which cells stay together after division, forming groups composed of 4 or 8 cell subunits. We show that spherical fission yeast can rapidly evolve multicellular clusters with cuboidal organization under size-based selection, and that these clusters exhibit key features of an evolutionary transition in individuality. We also find that mutations in the *ace2* gene, which prevents cell separation after division, are responsible for this phenotype in two independent lineages. Remarkably, *ace2* mutations also underlie the transition to multicellularity in budding yeast, a distantly related lineage. Our findings illustrate the simplicity and convergence of the genetic and biophysical factors that enable the origin of multicellular groups and life cycles, and shed light on the evolution of multicellularity via cuboidal cell packing across the tree of life.

Supplementary material

Supplementary material is available online at *Evolution Letters*. Supplementary material contain (1) the full time-lapse microscopy from Figure 2A, and (2) an Excel file with four tables. Supplementary Table S1 contains information on the taxa chosen to build the cladogram in Figure 1. The mutations identified in the spherical ancestor are listed in Supplementary Table S2. The mutations identified in the 334-day evolved populations and the GO enrichment analysis results can be found in Supplementary Tables S3 and S4.

Data and code availability

All scripts and raw data are available at https://github.com/Ratcliff-Lab/pombe-paper. Raw Illumina sequencing reads are available at the NIH Sequence Read Archive under accession number PRJNA1106067.

Author contributions

R.M.P., G.O.B., and W.C.R. conceived the project. R.M.P., G.O.B., P.C.K., D.T.L., M.G.D., T.E.R.B., and W.W. conducted the experiments. R.M.P. analyzed the data and generated the figures. R.M.P., G.O.B., and W.C.R. wrote the manuscript.

Funding

This work is supported by the National Science Foundation, Division of Environmental Biology (grant no. DEB-1845363).

Conflict of interest: The authors declare no conflict of interest.

Acknowledgments

We are grateful to Matthias Sipiczki, for sending us the spherical *S. pombe* ancestor. We would like to thank the Ratcliff lab for thoughtful discussions in the preparation of this manuscript as well as the GT QBioS Graduate Program for its support.

References

Anderson, R. P., Macdonald, F. A., Jones, D. S., McMahon, S., & Briggs, D. E. (2017). Doushantuo-type microfossils from latest ediacaran phosphorites of northern Mongolia. *Geology*, *45*(12), 1079–1082.

Barnett, D. W., Garrison, E. K., Quinlan, A. R., Strömberg, M. P., & Marth, G. T. (2011). Bamtools: A c++ api and toolkit for analyzing and managing bam files. *Bioinformatics*, *27*(12), 1691–1692.

Bernardes, J. P., John, U., Woltermann, N., Valiadi, M., Hermann, R. J., & Becks, L. (2021). The evolution of convex trade-offs enables the transition towards multicellularity. *Nature Communications*, *12*(1), 4222.

Bozdag, G. O., Zamani-Dahaj, S. A., Day, T. C., Kahn, P. C., Burnetti, A. J., Lac, D. T., Tong, K., Conlin, P. L., Balwani, A. H., Dyer, E. L., Yunker, P. J., & Ratcliff, W. C. (2023). De novo evolution of macroscopic multicellularity. *Nature*, *617*(7962), 747–754.

Chen, S., Zhou, Y., Chen, Y., & Gu, J. (2018). fastp: An ultra-fast all-in-one fastq preprocessor. *Bioinformatics*, *34*(17), i884–i890.

Cingolani, P., Platts, A., Wang, L. L., Coon, M., Nguyen, T., Wang, L., Land, S. J., Lu, X., & Ruden, D. M. (2012). A program for annotating and predicting the effects of single nucleotide polymorphisms, snpeff: Snps in the genome of *Drosophila melanogaster* strain w1118; iso-2; iso-3. *fly*, *6*(2), 80–92.

Danecek, P., Auton, A., Abecasis, G., Albers, C. A., Banks, E., DePristo, M. A., Handsaker, R. E., Lunter, G., Marth, G. T., Sherry, S. T., McVean, G., & Richard, D. (2021). The variant call format and vcftools. *Bioinformatics*, *27*(15), 2156–2158.

Day, T. C., Höhn, S. S., Zamani-Dahaj, S. A., Yanni, D., Burnetti, A., Pentz, J., Honerkamp-Smith, A. R., Wioland, H., Sleath, H. R., Ratcliff, W. C., Goldstein, R. E., & Yunker, P. J. (2022). Cellular organization in lab-evolved and extant multicellular species obeys a maximum entropy law. *Elife*, *11*, e72707.

DiMaio, M. A., Park, W. G., & Longacre, T. A. (2014). Gastric sarcina organisms in a patient with cystic fibrosis. *Human Pathology: Case Reports*, *1*(3), 45–48.

Driscoll, W. W., & Travisano, M. (2017). Synergistic cooperation promotes multicellular performance and unicellular free-rider persistence. *Nature Communications*, *8*(1), 15707.

Dudin, O., Wielgoss, S., New, A. M., & Ruiz-Trillo, I. (2022). Regulation of sedimentation rate shapes the evolution of multicellularity in a close unicellular relative of animals. *PLoS Biology*, *20*(3), e3001551.

García, P., Tajadura, V., García, I., & Sánchez, Y. (2006). Rgf1p is a specific rho1-gef that coordinates cell polarization with cell wall biogenesis in fission yeast. *Molecular Biology of the Cell*, *17*(4), 1620–1631.

Godfray, H. C. J., & May, R. M. (2014). Open questions: Are the dynamics of ecological communities predictable? *BMC Biology*, *12*(1), 1–3.

Godfrey-Smith, P., Bouchard, F., & Huneman, P. (2013). Darwinian individuals. In F. Bouchard, & P. Huneman (Eds.), *From groups to individuals: Evolution and emerging individuality* (pp. 16–17). MIT Press.

Grosberg, R. K., & Strathmann, R. R. (2007). The evolution of multicellularity: A minor major transition? *Annual Review of Ecology, Evolution, and Systematics*, *38*, 621–654.

Jacobeen, S., Pentz, J. T., Graba, E. C., Brandys, C. G., Ratcliff, W. C., & Yunker, P. J. (2018). Cellular packing, mechanical stress and the evolution of multicellularity. *Nature Physics*, *14*(3), 286–290.

Kamran, M., Calcagno, A.-M., Findon, H., Bignell, E., Jones, M. D., Warn, P., Hopkins, P., Denning, D. W., Butler, G., Rogers, T., Mühlschlegel, F. A., & Haynes, K. (2004). Inactivation of transcription factor gene ace2 in the fungal pathogen candida glabrata results in hypervirulence. *Eukaryotic Cell*, *3*(2), 546–552.

King, N., Westbrook, M. J., Young, S. L., Kuo, A., Abedin, M., Chapman, J., Fairclough, S., Hellsten, U., Isogai, Y., Letunic, I., Marr, M., Pincus, D., Putnam, N., Rokas, A., Wright, K. J., Zuzow, R., Dirks, W., Good, M., Goodstein, D., … Rokhsar, D. (2008). The genome of the choanoflagellate *Monosiga brevicollis* and the origin of metazoans. *Nature*, *451*(7180), 783–788.

Kleunen, M. V., Fischer, M., & Schmid, B. (2002). Experimental life-history evolution: Selection on the allocation to sexual reproduction and its plasticity in a clonal plant. *Evolution*, *56*(11), 2168–2177.

Knoll, A. H. (2011). The multiple origins of complex multicellularity. *Annual Review of Earth and Planetary Sciences*, *39*, 217–239.

Kulkarni, P., Behal, A., Mohanty, A., Salgia, R., Nedelcu, A. M., & Uversky, V. N. (2022). Co-opting disorder into order: Intrinsically disordered proteins and the early evolution of complex multicellularity. *International Journal of Biological Macromolecules*, *201*, 29–36.

Lenski, R. E., Rose, M. R., Simpson, S. C., & Tadler, S. C. (1991). Long-term experimental evolution in *Escherichia coli*. I. Adaptation and divergence during 2,000 generations. *The American Naturalist*, *138*(6), 1315–1341.

Li, H. (2013). Aligning sequence reads, clone sequences and assembly contigs with bwa-mem. *arXiv preprint arXiv:1303.3997*.

Li, H., Handsaker, B., Wysoker, A., Fennell, T., Ruan, J., Homer, N., Marth, G., Abecasis, G., Durbin, R., & Subgroup, G. P. D. P. (2009). The sequence alignment/map format and samtools. *Bioinformatics*, *25*(16), 2078–2079.

Mitchison-Field, L. M., Vargas-Muñiz, J. M., Stormo, B. M., Vogt, E. J., Van Dierdonck, S., Pelletier, J. F., Ehrlich, C., Lew, D. J., Field, C. M., & Gladfelter, A. S. (2019). Unconventional cell division cycles from marine-derived yeasts. *Current Biology*, *29*(20), 3439–3456.

Murray, J. M., Watson, A. T., & Carr, A. M. (2016). Transformation of Schizosaccharomyces pombe: Lithium acetate/dimethyl sulfoxide procedure. *Cold Spring Harbor Protocols*, *2016*(4), pdb–prot090969.

Niklas, K. J., Wayne, R., Benítez, M., & Newman, S. A. (2019). Polarity, planes of cell division, and the evolution of plant multicellularity. *Protoplasma*, *256*, 585–599.

Olson, B. J., & Nedelcu, A. M. (2016). Co-option during the evolution of multicellular and developmental complexity in the volvocine green algae. *Current Opinion in Genetics & Development*, *39*, 107–115.

Pentz, J. T., MacGillivray, K., DuBose, J. G., Conlin, P. L., Reinhardt, E., Libby, E., & Ratcliff, W. C. (2023). Evolutionary consequences of nascent multicellular life cycles. *eLife*, 12, e84336.

Proeschold, T., & Darienko, T. (2020). The green puzzle stichococcus (trebouxiophyceae, chlorophyta): New generic and species concept among this widely distributed genus. *Phytotaxa*, 441(2), 113–142.

Ratcliff, W. C., Denison, R. F., Borrello, M., & Travisano, M. (2012). Experimental evolution of multicellularity. *Proceedings of the National Academy of Sciences*, *109*(5), 1595–1600.

Ratcliff, W. C., Fankhauser, J. D., Rogers, D. W., Greig, D., & Travisano, M. (2015). Origins of multicellular evolvability in snowflake yeast. *Nature Communications*, *6*(1), 6102.

Ratcliff, W. C., Herron, M. D., Howell, K., Pentz, J. T., Rosenzweig, F., & Travisano, M. (2013). Experimental evolution of an alternating uni-and multicellular life cycle in *Chlamydomonas reinhardtii*. *Nature Communications*, *4*(1), 2742.

Raudvere, U., Kolberg, L., Kuzmin, I., Arak, T., Adler, P., Peterson, H., & Vilo, J. (2019). g: Profiler: A web server for functional enrichment analysis and conversions of gene lists (2019 update). *Nucleic Acids Research*, *47*(W1), W191–W198.

Robinson, J. T., Thorvaldsdóttir, H., Turner, D., & Mesirov, J. P. (2023). igv. js: An embeddable javascript implementation of the integrative genomics viewer (igv). *Bioinformatics*, *39*(1), btac830.

Rose, C. J., & Hammerschmidt, K. (2021). What do we mean by multicellularity? The evolutionary transitions framework provides answers. *Frontiers in Ecology and Evolution*, *9*, 730714.

Sipiczki, M. (2000). Where does fission yeast sit on the tree of life? *Genome Biology*, *1*(2), 1–4.

Sipiczki, M., Yamaguchi, M., Grallert, A., Takeo, K., Zilahi, E., Bozsik, A., & Miklos, I. (2000). Role of cell shape in determination of the division plane in Schizosaccharomyces pombe: Random orientation of septa in spherical cells. *Journal of Bacteriology*, *182*(6), 1693–1701.

Spitze, K. (1993). Population structure in *Daphnia obtusa*: Quantitative genetic and allozymic variation. *Genetics*, *135*(2), 367–374.

Suga, H., Chen, Z., De Mendoza, A., Sebé-Pedrós, A., Brown, M. W., Kramer, E., Carr, M., Kerner, P., Vervoort, M., Sánchez-Pons, N., Torruella, G., Derelle, R., Manning, G., Lang, F., B., Russ, C., Haas, B. J., Roger A. J., Nusbaum, C., & Ruiz-Trillo, I. (2013). The capsaspora genome reveals a complex unicellular prehistory of animals. *Nature Communications*, *4*(1), 2325.

Umen, J., & Herron, M. D. (2021). Green algal models for multicellularity. *Annual Review of Genetics*, 55, 603–632.

Van der Auwera, G. A., Carneiro, M. O., Hartl, C., Poplin, R., Del Angel, G., Levy-Moonshine, A., Jordan, T., Shakir, K., Roazen, D., Thibault, J., Banks, E., Garimella, K., V., Altshuler, D., Gabriel, S., & DePristo, M., A. (2013). From fastq data to highconfidence variant calls: The genome analysis toolkit best practices pipeline. *Current Protocols in Bioinformatics*, *43*(1), 11–10.

Xiao, S., Muscente, A., Chen, L., Zhou, C., Schiffbauer, J. D., Wood, A. D., Polys, N. F., & Yuan, X. (2014). The weng'an biota and the ediacaran radiation of multicellular eukaryotes. *National Science Review*, *1*(4), 498–520.

Xiao, S., Zhang, Y., & Knoll, A. H. (1998). Three-dimensional preservation of algae and animal embryos in a neoproterozoic phosphorite. *Nature*, *391*(6667), 553–558.

Yund, P. O., Marcum, Y., & Stewart-Savage, J. (1997). Life-history variation in a colonial ascidian: Broad-sence heritabilities and tradeoffs in allocation to asexual growth and male and female reproduction. *The Biological Bulletin*, *192*(2), 290–299.